Chapter 5

Development of donor-acceptor architecture-based theranostic fluorescent probes

Chapter 5

Development of donor-acceptor architecture-based theranostic fluorescent probes

5.1 Design strategy

The design of promising theranostic agents demands a rational structural framework constructed with composition of two key functionalities i.e., a lead therapeutic scaffold and a biomarker labeling moiety. Accordingly, the novel theranostic agents were designed with the amalgamation of prominent structural features from the anti-AD therapeutic classes and fluoroprobes with the electron donor-acceptor architecture **(Figure 5.1)** for the simultaneous detection of the Aβ species and inhibit the cholinesterase (ChEs) enzymes, which are primary targets for the development of therapeutics for the AD (18). The push-pull architecture of the theranostic agents were constructed by utilizing indolium and benzothiazolium as electron-acceptor (A) groups combined with electron donating (D), *N*-aryl piperazine scaffold linked by conjugated π-electron containing benzylidene moiety as backbone structure (148). The photophysical characteristic can be achieved with the ICT phenomenon between electron-deficient, indolium or benzothiazolium moiety and strong electron-donating, *N,N′*-dimethylamino group in the piperazine scaffold through aromatic π bridge (120). In addition to the diverse pharmacological activities, promising aspect of indolium (153) and benzothiazole scaffold (128) as fluorescent imaging agents, including, association with large stokes shift, high fluorescence quantum yield, low toxicity, good biocompatibility, and excellent photostability were widely applied for the diagnosis of various diseases or disorders by monitoring essential biomarkers (154, 155). Several indolium and benzothiazole based derivatives have been designed and reported to detect the AD biomarkers. The report by Chan H. *et al.* advocated indolium-based turn-on fluorophore, **SIM** for the detection of different biomarkers including, Aβ peptide, tau, and phosphorylated tau for the diagnosis of AD. In the presence of **SIM**, an exceptionally low limit of detection down to the femto-molar level was achieved in the assay (156). Gu *et al.* described water soluble 2-

styrylindolium-based fluorescent probes for the visualization of NFTs in the AD. Compounds, *2-[2-[4-(1-pyrrolidinyl)phenyl]ethenyl]-1,3,3-trimethyl-3H-indolium iodide* (**STY**) and *2-[2-[4-(diethylamino)phenyl]ethenyl]-1-butyl-3,3-dimethyl-3H-indolium iodide* exhibited excellent binding affinities to tau-aggregates (157). Li F. *et al*. developed the mitochondria-specific aggregation induced emission (AIE) probe, **TPE-Ph-In** to observe the protective effect of curcumin micelles on the damage of mitochondrial morphology, distribution, and membrane potential caused by Aβ (158). A NIR fluorescence probe employed with chromene-indolium (**Chy**) was developed by Yang *et al.* for the detection of endogenous BChE activity, widely distributed in the cerebral cortex and overexpressed in hippocampal neurons in AD mouse models (159). Wang *et al.* developed unique benzothiazolium derivative-capped silica nanocomposites based on ThT for Aβ imaging. The nanocomposites (**MSN-Lf@SZIs**) were able to deliver the design fluorescent probes into the brain of AD mouse and image Aβ species (82). The push-pull benzothiazole derivative, **PP-BTA-4** reported by Ono M. *et al.* as fluorescent probes demonstrated significant fluorescence characteristics and affinity towards the $A\beta_{1-42}$ and α-syn aggregates (160). The novel series of photo-triggered fluorescent probes for Aβ detection were also reported, where the probe transformed to weak fluorescent benzothiazole-coumarin structure under light irradiation by releasing the protecting group and cyclization reaction (**PTAD-3**). It generated the strong fluorescence complex on the binding of benzothiazole-coumarin with Aβ fibrils and successfully been applied to image Aβ plaques in the live AD mice (161). Wang *et al.* reported probe **BTS** containing Aβ-responsive benzothiazole aniline group and a dansyl group with environment sensitivity for dynamic *in situ* visualization of $A\beta_{40}$ species. It targeted selectively *N*-terminal region of Aβ with high sensitivity, thus causing the enhancement in the fluorescence response (139). The strong electron-donating potential

of *N*,*N*′-dimethylamino moiety has already been explored (162) and its existence in the piperazine moiety made it bifunctional electron-donor system, and the advantage of that could be utilized to construct the fluorescent probes (121). The therapeutic potential in the designed probes can be accomplished with the presence of the substituted *N*-aryl piperazine scaffold, known to exhibit anti-AD therapeutic potential and neuronal protection (113, 123). The piperazine containing compounds have been reported for the strong inhibition against AChE and BuChE, potential drug targets for AD (124).

In the present study, we report the synthesis, characteristics, and biological evaluations of the donor-acceptor type theranostic fluorescent probes for Aβ species and ChEs inhibition in AD.

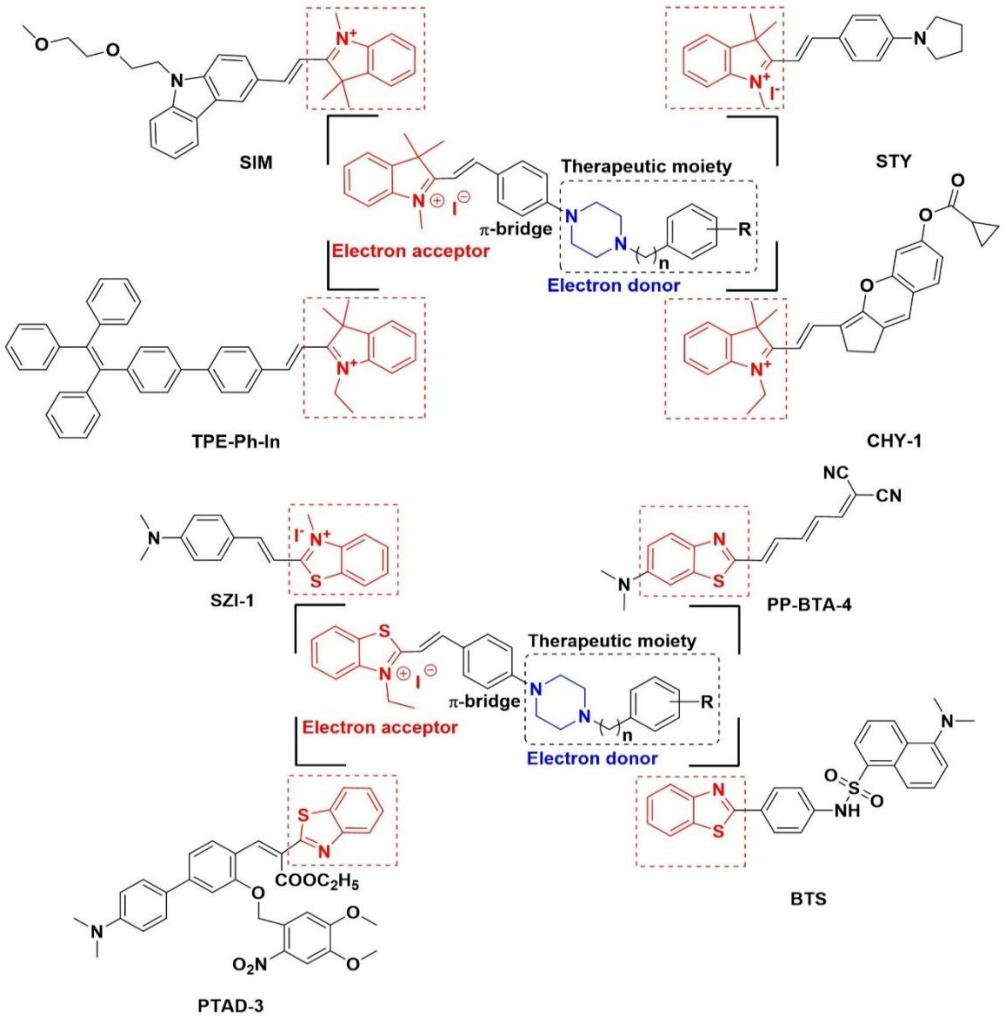

Figure 5.1. Molecular framework and design stratergy of donor-acceptor architecture type theranostic fluroscent probes.

5.2 Experimental procedures

5.2.1 Chemistry

All the chemicals and reagents used for the synthesis were sourced from commercial suppliers and were used as such without further purification, unless specified otherwise. The pre-coated silica gel 60 F254 thin-layer chromatography (TLC) plates were used to monitor the progress of the reactions. The spots were visualized under ultraviolet light or iodine vapours as needed. Melting points of synthesized compounds were determined on automated melting point apparatus (Barnstead Electrothermal, UK). Proton (^{1}H) and

carbon (^{13}C) NMR spectra were recorded on Bruker Advance, 500 MHz and 125 MHz spectrometers, respectively. NMR samples were prepared in DMSO-d_6 and $CDCl_3$ solvents at room temperature. Chemical shifts were reported in ppm (δ values) relative to tetramethylsilane (TMS) as the internal standard. The mass spectrum of the lead compound was obtained using the SCIEX X500R QTOF mass spectrometer, equipped with an APCI and ESI multimode ionization source (appendix).

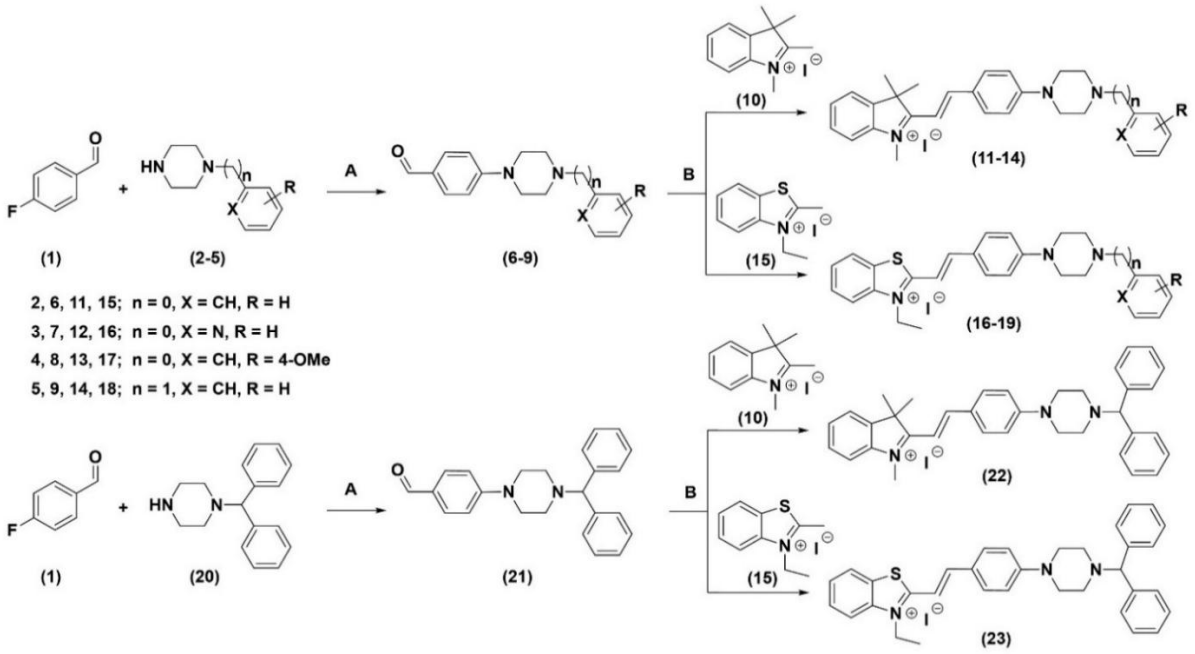

Scheme 5.1 Reagents and conditions: **A.** 4-fluorobenzaldehyde (**1**) 1.0 equiv, *N*-arylpiperazine (**2-5**) or 1-benzhydrylpiperazine (**20**) 1.0 equiv, potassium carbonate 2.0 equiv, DMF,125° C, 12 h**; B.** Intermediate (**6-9**/**21**) 1.0 equiv, *1,2,3,3-tetramethyl-3H-indolium iodide* (**10**) or *3-ethyl-2-methylbenzo[d]thiazol-3-ium iodide* (**15**) 1.5 equiv, 0.2 mL of piperidine, ACN, reflux, 80 ° C, 5-6 h.

5.2.1.1 General procedure for the synthesis of 6-9 & 21

To the reaction mixture of 4-fluorobenzaldehyde (**1**) (1.0 equiv) and anhydrous potassium carbonate (K_2CO_3) (2.0 equiv) in 5 mL of dimethylformamide (DMF), appropriate substituted piperazine (**2-5/20**) (1.0 equiv) were added. The resultant mixture, in a round-bottomed (R.B) flask with stirring, was refluxed for 12h at 125°C. The reaction progress

was monitored by TLC with the mobile phase, ethyl acetate, and hexane (4:6). After completion of the reaction, the mixture was poured in ice water. The solid formed was filtered, washed with water and petroleum ether to obtain pure product (**6-9**/**21)** in excellent yields.

5.2.1.2 General procedure for the synthesis of compounds 11-14; 16-19 & 22-23.

A solution of substituted intermediate (**6-9**/**21**) (1.5 equiv) and appropriate 1,2,3,3-tetramethyl-3H-indolium iodide (**10**) or -ethyl-2-methylbenzo[d]thiazol-3-ium iodide (**15**), (1.5 equiv) in acetonitrile (ACN) were taken in a 50-mL R.B flask. Piperidine solution was added dropwise in a catalytic amount (0.2 mL). Then the reaction mixture was refluxed at 80°C for 5-6h. After cooling to room temperature, the mixture was dried in vacuum. The product was purified by reprecipitation with diethyl ether (three times) to afford desired derivatives **11-14; 16-19** & **22-23.**

(E)-1,3,3-Trimethyl-2-(4-(4-phenylpiperazin-1-yl)styryl)-3H-indol-1-ium iodide **(11):** Dark brown solid, yield: 82 %. ^{1}H NMR (500 MHz, DMSO-d_6) δ 8.33 (d, J = 15.8 Hz, 1H), 8.12 (d, J = 9.0 Hz, 2H), 7.81 (d, J = 6.9 Hz, 1H), 7.76 (d, J = 7.9 Hz, 1H), 7.58 (t, J = 8.3 Hz, 1H), 7.52 (t, J = 7.4 Hz, 1H), 7.36 (d, J = 15.9 Hz, 1H), 7.29 – 7.24 (m, 2H), 7.17 (d, J = 9.2 Hz, 2H), 7.01 (d, J = 7.9 Hz, 2H), 6.83 (t, J = 7.2 Hz, 1H), 4.02 (s, 3H), 3.75 – 3.69 (m, 4H), 3.31 (m, 4H), 1.77 (s, 6H). MS (ESI+): *m/z* calculated for $C_{29}H_{32}N_3^+$: 422.2591; found: 422.2607.

(E)-1,3,3-trimethyl-2-(4-(4-(pyridin-2-yl)piperazin-1-yl)styryl)-3H-indol-1-ium iodide **(12):** Reddish brown solid, yield: 78%. ^{1}H NMR (500 MHz, DMSO-d_6) δ 8.33 (d, J = 15.8 Hz, 1H), 8.12 (d, J = 8.8 Hz, 2H), 7.80 (d, J = 7.1 Hz, 1H), 7.77 – 7.73 (m, 3H), 7.58 (td, J = 7.6, 1.3 Hz, 1H), 7.36 (d, J = 15.9 Hz, 1H), 7.18 (d, J = 8.9 Hz, 2H), 7.01 – 6.96 (m, 2H), 6.87 (td, J = 7.5, 1.5 Hz, 1H), 4.02 (s, 3H), 3.71 (m, 4H), 3.17 (m, 4H), 1.77 (s, 6H). MS (ESI+): *m/z* calculated for $C_{28}H_{31}N_4^+$: 423.2543; found: 423.2577.

(E)-2-(4-(4-(4-Methoxyphenyl)piperazin-1-yl)styryl)-1,3,3-trimethyl-3H-indol-1-ium iodide **(13):** Brown to red solid, yield: 84 %. ^{1}H NMR (500 MHz, DMSO-d_6) δ 8.33 (d, J = 15.9 Hz, 1H), 8.16 (d, J = 3.6 Hz, 1H), 8.13 (d, J = 8.7 Hz, 2H), 7.81 (d, J = 7.3 Hz, 1H), 7.75 (d, J = 7.9 Hz, 1H), 7.58 (q, J = 7.1, 6.6 Hz, 2H), 7.52 (t, J = 7.4 Hz, 1H), 7.35

(d, *J* = 15.9 Hz, 1H), 7.15 (d, *J* = 8.8 Hz, 2H), 6.89 (d, *J* = 8.5 Hz, 1H), 6.73 – 6.65 (m, 1H), 4.02 (s, 3H), 3.71 (s, 8H), 1.77 (s, 6H). MS (ESI+): *m/z* calculated for $C_{30}H_{34}N_3O^+$: 452.2696; found: 452.2718.

***(E)-2-(4-(4-Benzylpiperazin-1-yl)styryl)-1,3,3-trimethyl-3H-indol-1-ium iodide* (14):** Dark brown solid, yield: 79 %. ^{1}H NMR (500 MHz, DMSO-d_6) δ 8.31 (d, *J* = 15.8 Hz, 1H), 8.09 (d, *J* = 9.0 Hz, 2H), 7.80 (d, *J* = 7.0 Hz, 1H), 7.75 (d, *J* = 7.9 Hz, 1H), 7.57 (t, *J* = 8.3 Hz, 1H), 7.51 (t, *J* = 7.5 Hz, 1H), 7.37 – 7.31 (m, 5H), 7.28 (s, 1H), 7.10 (d, *J* = 9.1 Hz, 2H), 4.02 (s, 3H), 3.56 (s, 6H), 3.34 (s, 4H), 1.76 (s, 6H). MS (ESI +): *m/z* calculated for $C_{30}H_{34}N_3^+$: 436.2747; found: 436.2728.

***(E)-2-(4-(4-Benzhydrylpiperazin-1-yl)styryl)-1,3,3-trimethyl-3H-indol-1-ium iodide* (22):** Brown to red solid, yield: 86 %. ^{1}H NMR (500 MHz, DMSO-d_6) δ 8.31 (d, *J* = 15.8 Hz, 1H), 8.08 (d, *J* = 8.8 Hz, 2H), 7.80 (d, *J* = 7.2 Hz, 1H), 7.75 (d, *J* = 8.0 Hz, 1H), 7.58 (t, *J* = 7.7 Hz, 1H), 7.52 (d, *J* = 7.5 Hz, 1H), 7.49 (d, *J* = 7.5 Hz, 4H), 7.33 (t, *J* = 6.9 Hz, 5H), 7.23 (t, *J* = 7.3 Hz, 2H), 7.07 (d, *J* = 8.9 Hz, 2H), 4.39 (s, 1H), 4.01 (s, 3H), 3.57 (s, 4H), 2.46 (s, 4H), 1.76 (s, 6H). MS (ESI +): *m/z* calculated for $C_{36}H_{38}N_3^+$: 512.3060; found: 512.3041.

***(E)-3-Ethyl-2-(4-(4-phenylpiperazin-1-yl)styryl)benzo[d]thiazol-3-ium iodide* (16):** Dark reddish solid, yield: 82 %. ^{1}H NMR (500 MHz, Chloroform-*d*) δ 8.36 (dd, *J* = 7.5, 1.6 Hz, 1H), 8.04 (dd, *J* = 7.5, 1.5 Hz, 1H), 7.73 (d, *J* = 7.5, 1.5 Hz, 1H), 7.55 (d, *J* = 7.5, 1.5 Hz, 1H), 7.46– 7.40 (m, 1H), 7.40 – 7.34 (m, 2H), 7.29 – 7.17 (m, 3H), 6.95 – 6.89 (m, 2H), 6.86 (t, *J* = 7.5, 1.5 Hz, 1H), 6.72 – 6.66 (m, 2H), 4.73 – 4.56 (m, 2H), 3.34 (d, *J* = 1.6 Hz, 8H), 1.47 (t, *J* = 8.0 Hz, 3H). MS (ESI+): *m/z* calculated for $C_{27}H_{28}N_3S^+$: 426.1998; found: 426.1981.

***(E)-3-Ethyl-2-(4-(4-(4-methoxyphenyl)piperazin-1-yl)styryl)benzo[d]thiazol-3-ium iodide* (17):** Brown solid, yield: 78 %. ^{1}H NMR (500 MHz, Chloroform-*d*) δ 8.39 (dd, *J* = 7.5, 1.6 Hz, 1H), 8.01 (dd, *J* = 7.6, 1.5 Hz, 1H), 7.76 (d, *J* = 7.5, 1.6 Hz, 1H), 7.60 (d, *J* = 7.5, 1.5 Hz, 1H), 7.46 – 7.41 (m, 1H), 7.41 – 7.36 (m, 2H), 7.25 (d, *J* = 15.2 Hz, 1H), 6.92 (s, 4H), 6.74 – 6.68 (m, 2H), 4.73 – 4.56 (m, 2H), 3.79 (s, 3H), 3.37 – 3.26 (m, 8H), 1.51 – 1.46 (m, 3H). MS (ESI+): *m/z* calculated for $C_{28}H_{30}N_3OS^+$: 456.2104; found 456.2127.

***(E)-3-Ethyl-2-(4-(4-(pyridin-2-yl)piperazin-1-yl)styryl)benzo[d]thiazol-3-ium iodide* (18):** Dark brown solid, yield: 87 %. ^{1}H NMR (500 MHz, DMSO-d_6) δ 8.35 (d, *J* = 7.8 Hz, 1H), 8.23 – 8.07 (m, 3H), 7.99 (d, *J* = 8.3 Hz, 2H), 7.81 (t, *J* = 7.6 Hz, 1H), 7.72 (d,

J = 12.5 Hz, 2H), 7.59 (t, *J* = 7.1 Hz, 1H), 7.11 (d, *J* = 8.3 Hz, 2H), 6.89 (d, *J* = 8.4 Hz, 1H), 6.73 – 6.64 (m, 1H), 4.95 – 4.82 (m, 2H), 3.65 (d, *J* = 32.1 Hz, 8H), 1.45 (t, *J* = 6.7 Hz, 3H). MS (ESI+): *m/z* calculated for $C_{26}H_{27}N_4S^+$: 427.1951; found: 427.1944.

***(E)-2-(4-(4-Benzylpiperazin-1-yl)styryl)-3-ethylbenzo[d]thiazol-3-ium iodide* (19):** Reddish solid, yield: 76 %. ^{1}H NMR (500 MHz, DMSO-d_6) δ 8.43 (dd, *J* = 7.5, 1.6 Hz, 2H), 8.02 (dd, *J* = 7.5, 1.5 Hz, 2H), 7.66 (d, *J* = 7.5, 1.6 Hz, 2H), 7.54 (d, *J* = 7.5, 1.6 Hz, 2H), 7.47 – 7.40 (m, 2H), 7.40 – 7.33 (m, 4H), 7.31 – 7.24 (m, 11H), 7.22 (s, 1H), 6.69 – 6.63 (m, 4H), 4.71 – 4.52 (m, 4H), 3.55 (s, 4H), 3.14 – 3.09 (m, 4H), 3.07 – 3.00 (m, 4H), 2.69 – 2.63 (m, 8H), 1.46 (t, *J* = 8.0 Hz, 6H). MS (ESI+): *m/z* calculated for $C_{28}H_{30}N_3S^+$: 440.2155: found: 440.2147.

***(E)-2-(4-(4-Benzhydrylpiperazin-1-yl)styryl)-3-ethylbenzo[d]thiazol-3-ium iodide* (23):** Brown red solid, yield: 85 %. ^{1}H NMR (500 MHz, DMSO-d_6) δ 8.35 (d, *J* = 7.7 Hz, 1H), 8.19 (d, *J* = 8.3 Hz, 1H), 8.10 (d, *J* = 15.2 Hz, 1H), 7.94 (d, *J* = 8.4 Hz, 2H), 7.81 (t, *J* = 7.6 Hz, 1H), 7.71 (t, *J* = 12.8 Hz, 2H), 7.49 (d, *J* = 7.2 Hz, 4H), 7.33 (t, *J* = 7.3 Hz, 4H), 7.22 (t, *J* = 7.0 Hz, 2H), 7.03 (d, *J* = 8.5 Hz, 2H), 4.87 (d, *J* = 6.9 Hz, 2H), 4.37 (s, 1H), 3.49 (s, 4H), 2.46 (s, 4H), 1.44 (t, *J* = 6.8 Hz, 3H). MS (ESI+): *m/z* calculated for $C_{34}H_{34}N_3S^+$: 516.2468; found: 516 .2472.

5.2.2 Measurement of photophysical properties

LogP and BBB permeability were estimated by widely used pkCSM web-server (http://biosig.unimelb.edu.au/pkcsm/prediction). The fluorescence data, including the excitation and emission wavelengths, of all the synthesized probes were measured in DMSO. To assess the solvatochromism properties of lead probes **22** & **18**, fluorescence spectra of lead was recorded in different solvents with distinct polarity including, Toluene, DCM, THF, Methanol, ACN, DMF, DMSO and H_2O.

5.2.3 *In-vitro* cholinesterase inhibition

The cholinesterase inhibitory activities of all the synthesized probes were determined spectrometrically as per the previously reported protocol of modified Ellman colorimetric assay (126, 134). The cholinesterase enzymes, *ee*AChE (CAS No. 9001–08-1) and

*eq*BuChE (CAS No. 9000–81-5) were purchased from Sigma Aldrich. Donepezil (0.01–100 µM) was used as the positive control against, *ee*AChE and *eq*BuChE (163). Briefly, the stock concentrations of the test compounds **(11-14** & **22) (16-19** & **23)** were prepared in biological grade DMSO and further working concentrations were made in PBS to determine the inhibitory activities (IC_{50}). The assay involved the hydrolysis of thiolated substrates catalyzed by the cholinesterase to produce thiocholine. Further, it caused the reduction of the 5,5-dithio-bis-(2- nitrobenzoic acid) (DTNB) to produce the yellow colour product that was detected colorimetrically. The assay procedure involved the first step of incubation of test compounds (10 ul) or standard compound (10 ul) with the 50 µl of *ee*AChE (0.22 U/mL) or 50 µl of *eq*BuChE (0.06 U/mL) enzymes in 96-well plates at room temperature for the period of 30 min. Then, 30 µl of the substrate, viz. ATCI (15 mM) or BTCI (15 mM) was added, and the solution was incubated for an additional 30 min. Finally, 160 µl solution of DTNB (1.5 mM) was added to each of the well, and the absorbance at 412 nm was measured using a 96-well microplate reader on Synergy HTX multi-mode reader (BioTek, USA). The blank control was prepared with all the components except the enzyme. Donepezil was used as a positive control or reference in the study. The assay was carried out in triplicate and experiments were repeated independently at least two to three times. The percentage inhibition of enzyme for each of the test compounds was calculated using the following equation: $[(Ac - Ai)/Ac] \times 100$, where Ai is the absorbance in the presence of the inhibitors and Ac is the absorbance in the absence of the inhibitors.

5.2.4 *In vitro* binding studies with $A\beta_{1-42}$ aggregates

The $A\beta_{1-42}$ peptide was purchased from Cayman (India) for the assay. The stock solution of 1 mg/mL of $A\beta_{1-42}$ was prepared by dissolving lyophilized aliquot of $A\beta_{1-42}$ in 80 µl of 1% NH_4OH and sterile PBS (920 µL, pH 7.4) and was stored at - 80°C. Further dilutions

were made with PBS solution to prepare a working solution of $A\beta_{1-42}$ peptide for experimentation (63). $A\beta_{1-42}$ monomers were incubated for 72h to prepare aggregated form of $A\beta_{1-42}$ peptide and the aggregation degree of $A\beta_{1-42}$ peptide was accessed by ThT fluorescence assay. The fluorescent characteristics of free probe **22/18** in the aqueous solution to their fluorescence properties in the presence of $A\beta_{1-42}$ monomers and $A\beta_{1-42}$ aggregates were determined. The final solution mixture of probe vs. $A\beta_{1-42}$ peptide was taken in a ratio of 2:1. To the solutions of test probes (30 μL, 50 μM) in PBS (pH = 7.4) $A\beta_{1-42}$ (30 μL, 25 μM) peptide suspension in PBS (pH = 7.4) was added. To evaluate the change in the fluorescence response probe **22/18** (50 μM) was incubated for 30 min with monomer and aggregated form of $A\beta_{1-42}$ proteins. The resulting mixture was transferred to a 384-well plate black (n = 3), and the plate was subjected to fluorescence imaging using (BioTek Synergy H1M) fluorescence spectrophotometer.

5.2.5 *In vitro* saturation binding assay using $A\beta_{1-42}$ aggregates

A solution of $A\beta_{1-42}$ aggregates (final concentration of 50 μM) was mixed with different concentrations of **22/18** (0, 0.05, 0.10, 0.15, 0.25,0.50, 0.75, 1.00, 1.50 and 2.50 μM) and incubated at room temperature for 10 min (137). Fluorescence response of the resultant mixture was measured by a fluorescence spectrometer at respective emission maxima. The K_d binding curve was generated by software prism 5.0 with nonlinear one-site binding regression.

5.2.6 Aβ deposit fluorescence imaging in the *Drosophila* AD model

In the study, GAL4/UAS transcription activating, bipartite system was used. The GAL4/UAS system is a genetic tool that is used to knock down, knock out, and overexpress the gene of interest in the tissue of interest. The *GAL4* is a transcriptional activator that binds to *UAS* enhancer sequences found in DNA. It then recruits transcription machinery to the site to induce gene expression. We used *elavGaL4* as

control, which is a pan-neuronal specific GAL4 line and *elavGAL4>UAS Aβ* as experimental population. The *UAS Aβ* is the *Drosophila* stock has Bloomington stock no. 33774, which is a familial AD inducing *Drosophila* stock. The flies were maintained at 25ºC and food change was done every alternate day. The genetic cross was set between *elavGAL4* female and *UAS Aβ* male for experimental genotype and in between the *elavGAL4* female and male for control genotype.

5.2.6.1 Thioflavin T staining

The larvae from the F1 progeny of the parental generation, *elavGAL4>UAS Aβ* were used from experimental and control genotype, *elavGAL4*. The third instar larvae were selected for dissection. The brain was dissected in PBS (1X) and fixation was done in 4% paraformaldehyde for a duration of 25 min. The sample tissue was washed with PBS for 15 min each. This was followed by the incubation under Thioflavin T. The stock concentration used was 2 mM and working concentration was 10 µM. The samples were washed with PBS(1X) for 15 min each thrice. The brain tissue was mounted in DABCO and observed under confocal microscope (Zeiss Confocal microscope, Imager Z2).

5.2.6.2 Staining for Probe 18

Like Thioflavin staining assay, the larvae were reared from the experimental, *elavGAL4>UAS Aβ* and control genotype, *elavGAL4*. The brain sample of the third instar larvae were selected for dissection, in PBS (1X). This was followed by fixation in 4% paraformaldehyde for a duration of 25 min. The sample tissue was washed with PBS for 15 min each and samples were incubated in the Probe **18**. The stock concentration was 2 mM and working concentration was 10 µM. This concentration was like Thioflavin T concentration so that the comparison can be made. The samples were washed thrice with PBS(1X) for 15 min and tissue was mounted in DABCO. The brain samples were observed under confocal microscope.

5.2.7 *In vivo* biological evaluations

5.2.7.1 Animals, housing, and ethical approval

This study adhered to the guidelines established by the Committee for the Purpose of Control and Supervision of Experiments on Animals (CPCSEA) and was conducted with the approval of the Institutional Animal Ethical Committee (IAEC), Indian Institute of Technology (BHU), Varanasi, under the IAEC approval number: IIT(BHU)/IAEC/2024/II/057.

5.2.7.2 Acute oral toxicity studies

The acute oral toxicity of the most promising compound **18**, was assessed in female albino mice following the OECD guideline 423. The experimental protocol involved dividing the animals into two groups (n = 3). The control group received an oral administration of the vehicle alone, while the second group was administered a single dose of compound **18** (300 mg/kg, p.o.). The animals were monitored over the subsequent 14 days for any toxic symptoms, changes in body weight, food consumption, behavioral alternation, adverse reactions, and mortality. After 14-days observation period, the animals were sacrificed, and vital organs, including the brain, liver, kidneys, and heart, were carefully isolated. Tissue transverse sections (15 μm thick) were prepared using a cryostat, mounted on glass slides, stained with hematoxylin and eosin dyes, and examined under a microscope (Magnus MLX Plus India) at 10X magnification to evaluate histological changes.

5.2.7.3 Behavioural studies

5.2.7.3.1 Treatment protocols

A total of six groups of mice, each group comprising of six animals, were included in the experiment. The normal control group (vehicle-treated) received 10 mL/kg (p.o) of normal saline. The scopolamine-treated (amnesic) group was administered 3 mg/kg (i.p)

of scopolamine. The donepezil-treated group administered with 5 mg/kg (p.o) of DPZ. Test groups were treated with oral doses of compound **18** at 5 mg/kg, 10 mg/kg and 20 mg/kg, respectively. The dosing regimen continued for seven consecutive days. On the seventh day, 60 min after the last administration of DPZ or compound **18**, a 3 mg/kg (i.p) dose of scopolamine was administered to all animals except those in the vehicle-treated group. Thirty min after the scopolamine injection, cognitive performance behaviral studies was assessed.

5.2.7.3.2 Y-maze test

Lead compound **18** was assessed for its anti-amnesic effect using Y-maze behavioural model in mice, following standard protocols (133, 135). The Y-maze apparatus consisted of three arms of equal dimensions arranged in a Y-shape, labelled as A, B, and C for convenience. Each arm measured 15.5 cm in height, 6 cm in width, and 20 cm in length, with the arms connected at a 120° angle. The test was conducted over a 5 min duration for each mouse, during which the sequence and total number of arm entries were recorded after the animal was placed in one arm. An entry into any arm was considered complete when the mouse's hind paws were fully inside the arm, and alternations were defined as consecutive entries into three different arms. To eliminate olfactory cues between tests, the Y-maze apparatus was cleaned with 70% ethanol solution after each session. On the seventh day, the escape latency (in seconds) for each mouse was measured. Mice were allowed to explore the apparatus freely when initially placed at its center. The percentage of spontaneous alternation performance (% SAP) was calculated using a formula: % spontaneous alternation (SA) = [(number of alternations/total arm entries) − 2] X 100. The % SA shows the short-term memory in mice.

5.2.7.3.3 Novel object recognition (NOR) test

The study also included the evaluation of memory-enhancing potential of the lead compound using the novel object recognition (NOR) test in a mouse model (164, 165). The testing apparatus, constructed from Plexiglass in a box shape, measured 40 cm × 40 cm × 30 cm. Prior to testing, the mice were acclimated to the apparatus for 2 - 3 min a day before the experiment. During the sample phase, two identical objects were placed in opposite corners of the apparatus, and the mice were allowed to freely explore the environment. Exploration of the objects was defined as either physical contact or positioning the nose within 2 cm of the object. After 24h, the test phase began. In this phase, one of the identical objects was replaced with a novel object. Mice were once again allowed to explore the objects freely, and the time spent exploring the familiar object (F) and the novel object (N) was recorded. The discrimination index (D1) was calculated using the formula:

$$D1 = \frac{N - F}{N + F}$$

Where, D1 represents the discrimination index, N is the time spent exploring the novel object, and F is the time spent exploring the familiar object.

5.2.7.4 *Ex-vivo* biochemical analysis

After performing the *in vivo* behavioural experiments, the mice from each group were sacrificed by cervical dislocation. The brains were carefully removed, and the hippocampus and cortex regions were isolated. The brain regions were homogenized in 12.5 mM PBS buffer (5 mL) using a glass homogenizer and centrifuged at 7000 rpm for 30 min at 4 °C to obtain the supernatant. The supernatant collected was used to analyse various biochemical parameters. The acetylcholine (ACh) levels were measured using an ACh ELISA kit. The cholinergic marker, acetylcholinesterase (AChE) levels, was

determined through a modified Ellman's colorimetric assay method (113, 134). For this, 50 µL of the supernatant was incubated with 30 µL of freshly prepared 15 mM acetylthiocholine iodide (ATCI) for 30 min. Subsequently, 160 µL of 1.5 mM DTNB was added, and the absorbance was measured immediately at a wavelength of 415 nm. Additionally, the brain supernatant was used to evaluate the levels of catalase (CAT) and malondialdehyde (MDA). The assays were performed using ELISA kits from ELK Biotechnology, strictly following the manufacturer's instructions.

5.3 Results and discussions

5.3.1 Chemistry

The designed probes were synthesized as described in the scheme (**Scheme 5.1**). The first step was the nucleophilic substitution reaction of 4-fluorobenzaldehye **(1)** with substituted *N*-aryl piperazine (**2-5**) or 1-benzhydrylpiperazine (**20**) in the presence of a strong base, potassium carbonate (126) to give intermediates (**6-9**) and (**21**) respectively. In the second step, the obtained intermediates (**6-9**)/(**21**), containing free aldehyde group, reacted with *1,2,3,3-tetramethyl-3H-indolium iodide* (**10**) or *3-ethyl-2-methylbenzo[d]thiazol-3-ium iodide* (**15**) in the presence of piperidine in catalytic amount to get the target probes **(11-14** & **22) or (16-19** & **23)** via Knoevenagel condensation. The synthesized probes were characterized by ^{1}H NMR and HRMS (appendix) and the structures are presented in **Table 5.1**.

5.3.2 *In-vitro* cholinesterase inhibition

The inhibition of AChE can restore the depleted cholinergic function in AD by consequently increasing the availability of ACh at the synaptic cleft. BuChE is an enzyme that can compensate for AChE by hydrolyzing ACh. Therefore, the concurrent inhibition of both AChE and BuChE (ChEs) would be more beneficial for anti-AD agents (113).

All the synthesized compounds/probes **(11-14** & **22) (16-19** & **23)** were evaluated for their ChEs inhibitory activities using DPZ as a reference molecule. Considering the higher degree of sequence homology and lower cost compared with human enzymes, both the enzymes from the animal sources (AChE from electric eel, *ee*AChE, and BuChE from equine serum, *eq*BuChE) were utilized in the study (126). The inhibitory potencies of evaluated compounds against ChEs are included in **Table 5.1**. The indolium and benzothiazolium scaffold was retained as a fluorophore in the respective derivatives with major substitution at the piperazine ring. In the indolium-based tested derivatives **(11-14** & **22)**, compounds **14** & **22** pronounced inhibitory potential against both *ee*AChE and *eq*BuChE enzymes. Whereas, compounds **18** & **19** from the benzothiazolium containing derivatives **(16-19** & **23)** showed potent inhibitory profile among all the tested compounds. In both the series, the compounds containing one carbon linker, i.e., benzylpiperazine (**14** & **19**) exhibited potent inhibition of ChEs, compound **14** (*ee*AChE IC_{50} 0.468 ± 0.021 μM; *eq*BuChE IC_{50} = 1.049 ± 0.142 μM) and compound **19 (***ee*AChE IC_{50} = 0.461 ± 0.037 μM; *eq*BuChE IC_{50} = 1.367 ± 0.121 μM). Conversely, compounds without carbon linker, i.e., phenyl piperazine (**11**, **12**, **16** & **17**) showed comparatively weak ChEs inhibition activity. The substitution of the electron-donating group, -OCH_3, at the phenyl piperazine moiety, compounds **12** & **17** diminished the ChEs activity. The compounds containing 2-pyridine ring on piperazine moiety exhibits significant inhibition of ChEs including compound **13** (*ee*AChE IC_{50} = 0.610 ± 0.064 μM; *eq*BuChE IC_{50} = 3.636 ± 0.350 μM). Compound **18** (*ee*AChE IC_{50} = 0.172 ± 0.011 μM; *eq*BuChE IC_{50} = 1.376 ± 0.141 μM) exhibited the most potent dual inhibition among all the tested molecules, comparable to the standard reference DPZ (*ee*AChE IC_{50} = 0.076 ± 0.004 μM; *eq*BuChE IC_{50} = 1.131 ± 0.194 μM), which is primarily more selective for the AChE.

Table 5.1: Structures, and cholinesterase inhibitory potential of synthesized compounds.

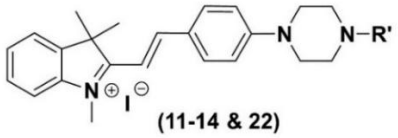

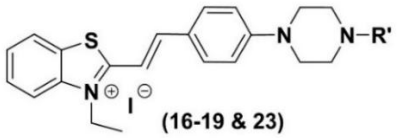

Compound ID	R`	IC_{50} (μM) [a] or % Inhibition[b] ± SD	
		*ee*AChE	*eq*BuChE
11	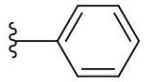	0.568 ± 0.108	2.113 ± 0.166
12	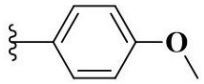	1.595 ± 0.148	44.24 ± 1.539 %
13	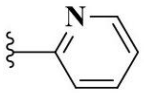	0.610 ± 0.064	3.636 ± 0.350
14	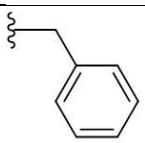	0.468 ± 0.021	1.049 ± 0.142
22	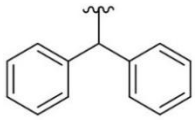	0.877 ± 0.092	4.870 ± 0.043
16	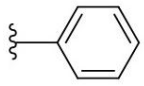	1.614 ± 0.1225	2.758 ± 0.053
17	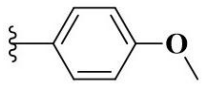	2.266 ± 0.013	5.089 ± 0.491
18	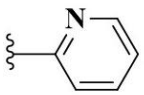	0.172 ± 0.011	1.376 ± 0.141
19	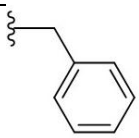	0.461 ± 0.037	1.367 ± 0.121
23	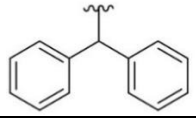	3.229 ± 0.120	2.894 ± 0.168
DPZ	**-**	0.076 ± 0.004	1.131 ± 0.194

[a]IC_{50}: 50% inhibitory concentration (mean ± standard deviation of two or three independent experiments). [b]% inhibition at a 20 μM concentration of inhibitors.

The results also indicated that the indolium-based derivatives bearing *N*-aryl benzylpiperazine scaffold (**22**) exhibited good inhibitory potential against *ee*AChE (IC_{50}= 0.877 ± 0.092 μM**)** and *eq*BuChE **(**IC_{50} = 4.870 ± 0.043 μM).

5.3.3 Measurement of photophysical properties

Log P values, BBB permeability and CNS permeability prediction and fluorescent properties, including, absorbance, excitation, and emission of all the probes were assessed (**Table 5.2**). The lipophilicity parameter is an important indicator of CNS penetration. A common measure of lipophilicity is the partition coefficient between *n*-octanol and water (log $P_{o/w}$). Notably, the predicted log P values for all the compounds tested ranged from 1.17 to 4.32. Compounds **22** & **23** has the higher lipophilic property with log P values > 4 comparable with standard DPZ. The ability of a drug to cross into the brain is an important parameter to improve the efficacy of drugs whose pharmacology activity is within the brain. For the given test compounds with logBB > 0.3 considered as it can readily cross the BBB, while compounds with logBB < -1 are poorly distributed to the brain (166). All the tested compounds except compound **11** showed the blood–brain permeability (BBB). Further, compounds **22** & **18** produced the highest permeation with logBB of 1.725 & 2.104 respectively.

In indolium-based derivatives, the excitation and emission wavelengths of compounds **11-14** & **22** were observed at 530/>600 nm in DMSO and 510/> 590 nm in PBS respectively (**Table 5.2**). Whereas, the excitation and emission wavelengths of benzothiazolium-based derivatives, **16-19** & **23** were observed at 510/>590 nm in DMSO and >450/590 nm in PBS respectively (**Figure 5.2**). To assess the sensitivity of D-π-A structure to the surrounding environmental polarity, fluorescence spectra of lead probes (**22** & **18**) was recorded in different solvents with distinct polarity including, Toluene, DCM, THF, Methanol, ACN, DMF, DMSO and H_2O. The solvent dependency changes have not been observed in the emission wavelength. Significant change in the fluorescence intensity was observed when moving from non-polar solvent such as toluene

to polar solvents such as DMSO and H_2O (**Figure 5.3**). The relative fluorescence quantum yield of probe **18** in methanol was measured to be 0.15.

Table 5.2: Photophysical properties of synthesized fluorescence probes**.**

Compound ID	Log P	BBB Permeability	λ_{abs} (nm) in DMSO	λ_{abs} (nm) in PBS	λ_{em} (nm) in DMSO	λ_{em} (nm) in PBS
11	1.17	0.241	530	510	600	590
12	2.74	0.994	530	510	600	590
13	2.13	0.747	530	510	600	590
14	2.73	1.535	530	510	610	590
22	4.32	1.725	530	510	610	600
16	2.70	1.319	510	460	590	590
17	2.71	0.965	510	460	590	590
18	2.10	2.104	510	470	610	590
19	2.70	1.486	510	450	610	590
23	4.29	1.676	510	490	610	600

The logP, and BBB Permeability were estimated by widely used pkCSM web-server (http://biosig.unimelb.edu.au/pkcsm/prediction), whereas λ_{abs} (nm) & λ_{em} (nm) were experimentally measured in DMSO & PBS.

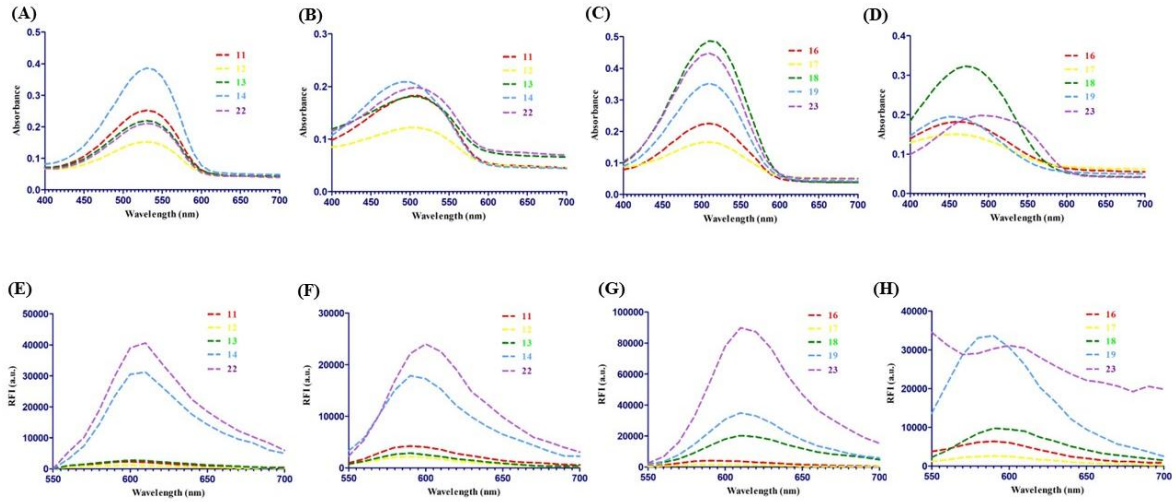

Figure 5.2. Absorbance spectra in DMSO **(A)** & PBS **(B)** and emission spectra in DMSO **(E)** & PBS **(F)** of indolium-based derivatives respectively. Absorption spectra in DMSO **(C)** & PBS **(D)** and emission spectra in DMSO **(G)** & PBS **(H)** of benzothiazolium-based derivatives, respectively.

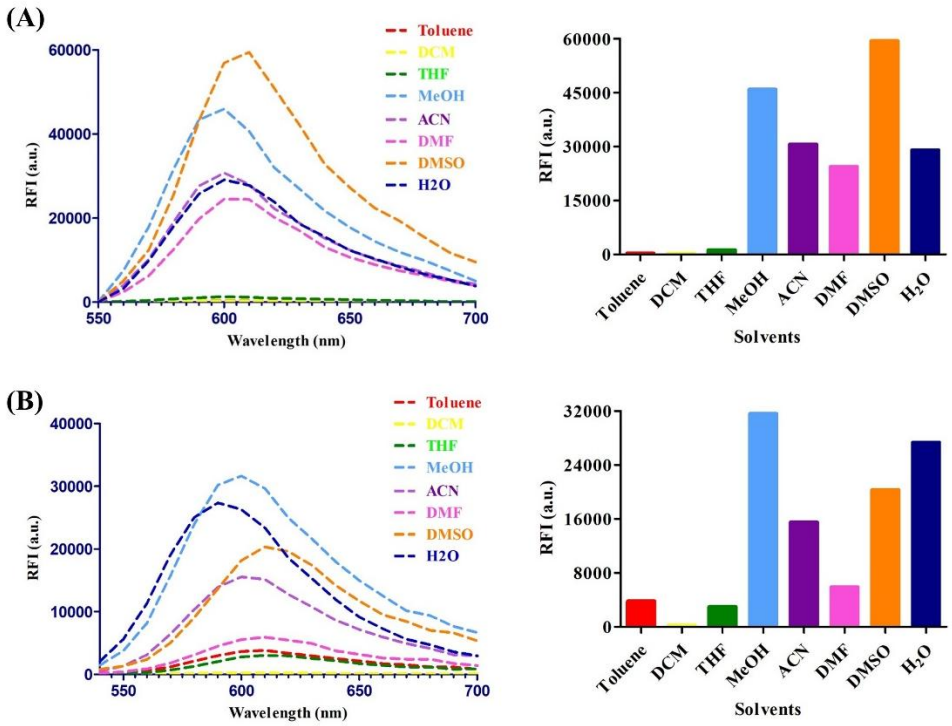

Figure 5.3. The fluorescence emission spectra of probes **22 (A)** and **18 (B)** in different solvents.

5.3.4 *In vitro* binding studies with $A\beta_{1-42}$ aggregates

The Aβ-binding fluorescent probes should exhibit a significant change in their spectral characteristics upon binding to Aβ species (114). On the incubation of probes **22** or **18** with $A\beta_{1-42}$ aggregates, the change in fluorescence response was observed (**Figure 5.4**). The fluorescent properties, including intensity and emission wavelength of free probes **22** and **18** in aqueous solution (PBS) were compared to their fluorescence properties in the presence of $A\beta_{1-42}$ monomers, $A\beta_{1-42}$ aggregates were compared. For both probes (**22** & **18**), a remarkable increase in the fluorescence intensity was observed when associated with $A\beta_{1-42}$ aggregates. The substantial enhancement in the fluorescence response may possibly be due to the binding of probes (**22** & **18**) with hydrophobic pockets of $A\beta_{1-42}$ aggregates and restricted mobility of compounds **22** & **18.** The findings also indicated that probes **22** and **18** would be "turned on" upon interacting with an $A\beta_{1-42}$ aggregates.

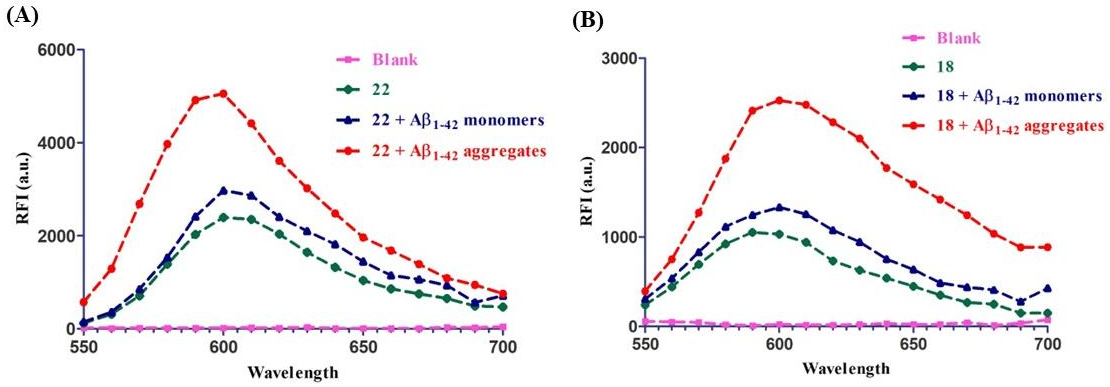

Figure 5.4. Change in fluorescence intensity of lead probes **22 (A)** and **18 (B)** upon interaction with $A\beta_{1-42}$ species.

5.3.5 In vitro saturation binding assay using $A\beta_{1-42}$ aggregates

The binding affinity of probes **22** & **18** with $A\beta_{1-42}$ aggregates was quantitatively evaluated with an *in vitro* saturation-binding assay (136, 137). The assay was conducted by the fluorescence titration measurement, and the binding constant (K_d) was determined through saturation assays. As shown in **Figure 5.5**, the nonlinear curve fitting revealed that the compounds **22** & **18** exhibited a high binding affinity toward $A\beta_{1-42}$ aggregates, with an apparent binding constant of K_d = 0.685 μM and K_d = 0.731 μM respectively. The obtained K_d is comparable to the previously reported benzothiazole-based fluorescent probes Ghosh S. *et al.* and Watanabe H. *et al.*, Where the K_d values of **RM-28** and **PP-BTA-4** for the $A\beta_{42}$ aggregate were found to be175.69 ± 4.87 nM and 40−148 nM, respectively (128, 160).

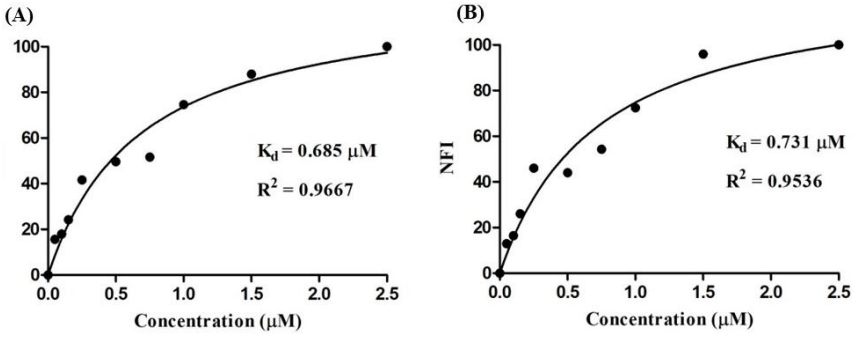

Figure 5.5. Binding constant of compounds **22 (A)** and **18 (B)** toward the $A\beta_{1-42}$ aggregates.

5.3.6 Aβ deposit fluorescence imaging in the *Drosophila* AD model

The GAL4/ UAS system is widely used to study the genetic interaction in *Drosophila* model. The system is used to for driving the expression of a gene of interest to a specific tissue thus over-expression, knock down and knock out of the gene of interest can be easily studied. In our study, we used *elavGAL4*, which is a pan-neuronal driver and UAS *Aβ* as gene of interest exhibiting AD in F1 progeny (*elavGAL4>UASAβ*). The female flies with *elavGAL4* in parental cross were crossed with UAS *Aβ* male flies, the F1 progeny expresses the Alzheimer's disease in the brain of *Drosophila*. The line used in the study is an early onset line (Bloomington no. 33774) thus express the gene in juvenile forms. The *in vivo* experiment in *Drosophila* model of AD, were performed on the larval brain tissue to detect the amyloid fibrils. It is known that Thioflavin T emits green fluorescence in presence of amyloid fibrils (167). Hence, we used it as control experiment stain. There is elevation in the staining intensity/pixel in the AD genotype, *elavGAL4>UAS Aβ* than control larval brain *elavGAL4* (**Figure 5.6**). We found that the Probe **18** exhibit fluorescence at λ_{ex} = 510–520 nm, and emission channel λ_{em} = 610–670 nm. There is significant elevation in fluorescence in *elavGAL4>UAS Aβ* larval brain samples than control *elavGAL4* larval brain (168, 169). The obtained results of Probe **18** staining are comparable to that of Thioflavin T assay; therefore, it indicated the ability to detect the Aβ aggregates in *elavGAL4>UAS Aβ*, *Drosophila* model for AD.

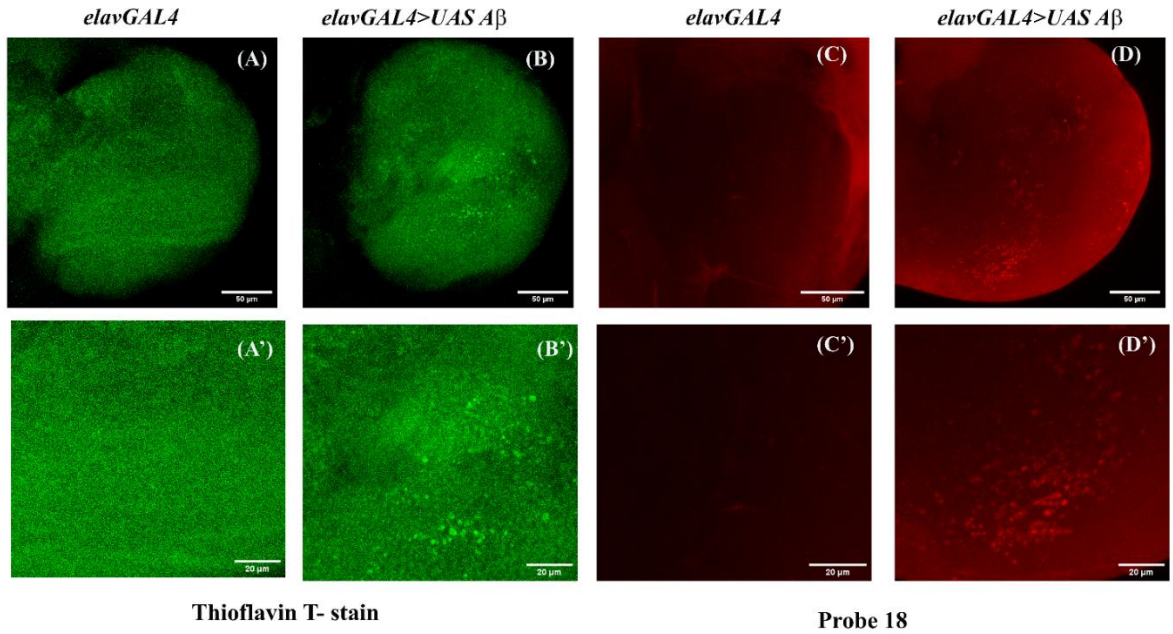

Figure 5.6. Confocal projection of larval brain in *Drosophila* larval brain **(A/A', B/B')** Intensity/pixel for thioflavin t staining, **A/A':** *elavGAL4*, control genotype and **B/B'**: *elavGAL4>UAS Aβ*, *Drosophila* model for AD (10 μM, λ_{ex} = 488 nm, and λ_{em} > 515 nm). **(C/C', D/D')** Intensity/pixel for compound Probe **22, C/C':** *elavGAL*4, control genotype and **D/D':** *elavGAL4>UAS Aβ*, *Drosophila* model for AD (10 μM, λ_{ex} = 510–520 nm, and λ_{em} = 610–670 nm) (n ≥ 10 biologically independent samples).

5.3.7 *In vivo* biological evaluations

5.3.7.1 Acute oral toxicity studies

The acute oral toxicity evaluation of the most promising compound **18**, was conducted in female mice following the OECD guideline 423 to evaluate its safety profile. The results indicated no signs or symptoms of toxicity, with no observed changes in body weight, food and water consumption, or mortality after the administration of compound **18**. Furthermore, histological examination revealed no damage to vital organs, including the brain, liver, heart, and kidneys, at doses up to 300 mg/kg, confirming the compound's safety at the tested dose (**Figure 5.7**).

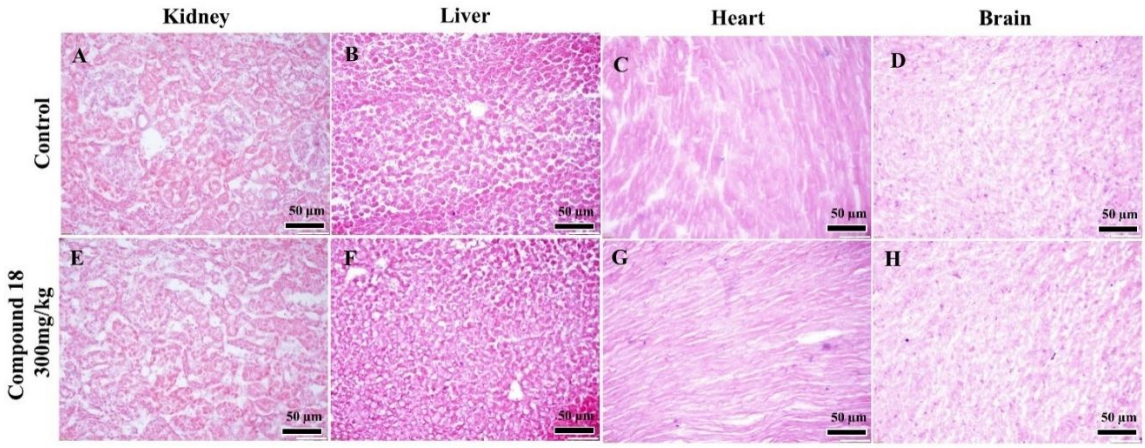

Figure 5.7. Effect of compound 18 on organ toxicity. (A–D) shows histological changes in the kidneys, liver, heart, and brain in the untreated control group. (E–H) illustrates the impact of compound 18 on histological changes in the kidneys, liver, heart, and brain, respectively.

5.3.7.2 Behavioural studies

5.3.7.2.1 Y-maze test

The Y-maze test results showed that the control group exhibited the highest percentage alternation, indicating intact spatial memory and cognitive function (**Figure 5.8)**. Scopolamine-treated group demonstrated a significant reduction in alternation percentage, reflecting cognitive impairment (123, 149, 150). Most importantly, the group treated with compound **18** at dose of 5 mg/kg partially restored alternation and found to be effective. Whereas, the treatment at dose of 10 & 20 mg/kg with the compound **18** significantly improved the alternation, achieving levels comparable to the group treated with DPZ, which also performed closely to the control group (152). In terms of the total number of arm entries, the control group showed the highest exploratory activity, while the scopolamine group exhibited a marked reduction, indicating impaired behaviour. Compound **18** treatment at all doses increased arm entries, with the 20 mg/kg dose showing the most substantial recovery, similar to the DPZ group.

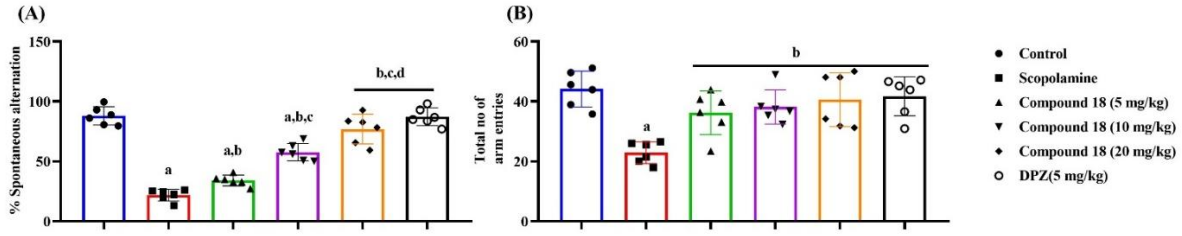

Figure 5.8. Effect of compound **18** and DPZ on cognitive improvement in the scopolamine-induced amnesia model **(A)** Represents the percentage of spontaneous alternation (**B**) Represents the total number of arm entries. $^{a}P < 0.05$ vs. control; $^{b}P < 0.05$ vs. scopolamine; $^{c}P < 0.05$ vs. compound **18** (5 mg/kg); $^{d}P < 0.05$ vs. compound **18** (10 mg/kg). One-way ANOVA followed by Newman - Keuls posthoc test.

5.3.7.2.2 Novel object recognition test

In NORT (164, 165), the control group exhibited the highest discrimination index, highlighting optimal cognitive function and intact recognition memory (**Figure 5.9)**. In contrast, the scopolamine-treated group showed a significant reduction in the discrimination index, indicating severe impairment in memory and recognition abilities. Treatment with compound **18** at dose of 5 mg/kg showed partial recovery, slightly improving the discrimination index compared to the scopolamine group. However, treatment with compound **18** at 10 mg/kg and 20 mg/kg doses demonstrated a more pronounced improvement. At dose of 20 mg/kg it showed the restoration of the discrimination index to levels comparable to the control group. Therefore, the 20 mg/kg dose of compound **18** exhibited nearly similar efficacy to DPZ, a standard cognitive enhancer, in reversing the scopolamine-induced memory deficits. The results suggested that compound **18**, especially at 20 mg/kg of dose, had strong neuroprotective and memory-enhancing properties, effectively mitigating scopolamine-induced cognitive impairment. This highlights its potential as a therapeutic candidate for conditions associated with memory deficits.

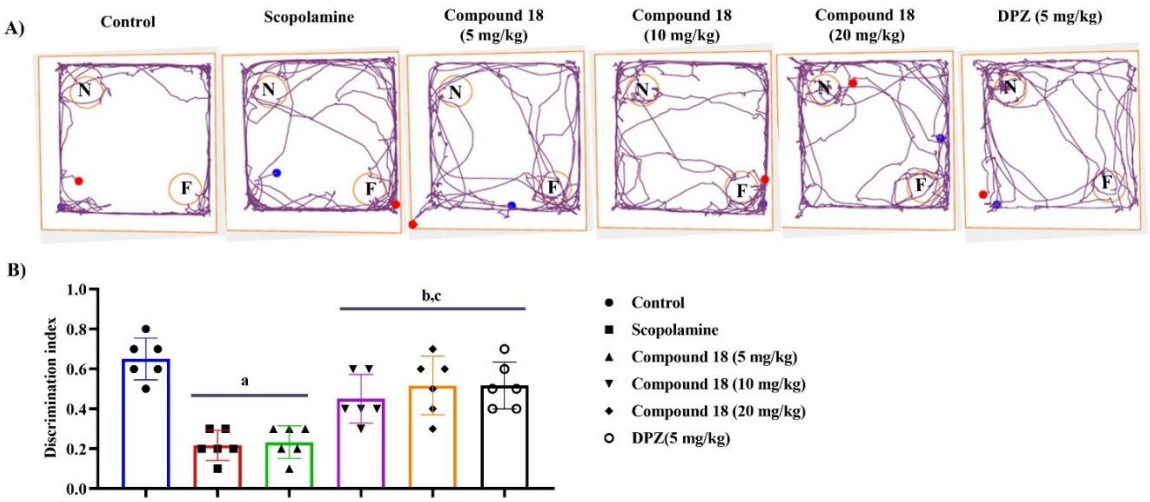

Figure 5.9. Novel object recognition test **(A)** Track plots & **(B)** Discrimination index between novel (**N**) and familiar (**F**) objects in control, scopolamine, and compound **18** treatment groups. The values were presented as the means ± SD. $^{a}P < 0.05$ vs. control; $^{b}P < 0.05$ vs. scopolamine; $^{c}P < 0.05$ vs. compound **18** (5 mg/kg). One-way ANOVA followed by Newman - Keuls posthoc test.

5.3.7.3 *Ex-vivo* biochemical analysis

The potential effects of compound **18** at the neurochemical levels were evaluated by measuring the levels of ACh and AChE (134), as well as other biochemical parameters like malondialdehyde (MDA) and catalase (CAT) (**Figure 5.10)**. Following the behavioural assessment, the mice from each of the groups were decapitated, and the hippocampus region of the brain was isolated and homogenized for further analysis. The results of this study demonstrated that the control group exhibited the highest levels of acetylcholine (ACh), reflective of normal cognitive function. In contrast, the scopolamine-treated group showed a significant reduction in ACh levels, consistent with cholinergic dysfunction and impaired cognitive performance. Treatment with compound **18** at doses of 5 mg/kg and 10 mg/kg partially restored ACh levels, whereas, at the dose of 10 mg/kg exhibited better efficacy. Notably, administration of compound **18** at 20 mg/kg and DPZ (5 mg/kg) significantly improved ACh levels. AChE activity was lower

in the control group, indicative of normal cholinergic signaling. Scopolamine administration indicated elevation in AChE activity, showed the disruption of the cholinergic system. However, treatment with compound **18** significantly reduced AChE level in dose dependent manner. whereas, at the 20 mg/kg dose it exhibited the most pronounced reduction, which was similar to the DPZ treatment. Furthermore, MDA levels, a key marker of oxidative stress, were significantly elevated in the scopolamine group, indicating increased lipid peroxidation and oxidative damage. Treatment with compound **18** resulted in a significant reduction in MDA levels, with the 20 mg/kg dose demonstrating the greatest efficacy. Similarly, DPZ treatment substantially decreased MDA levels indicating its antioxidant properties. CAT activity, a crucial indicator of antioxidant defence, was highest in the control group. The scopolamine group exhibited a substantial reduction in CAT activity, suggesting compromised antioxidant effect. The treatment with compound **18** and DPZ effectively improved CAT activity, with the 20 mg/kg dose of compound **18** and DPZ achieving the most significant recovery of antioxidant capacity. Scopolamine administration caused significant biochemical and oxidative changes. Compound **18**, particularly at a dose of 20 mg/kg, effectively ameliorated the alternations. Its neuroprotective and cognitive-enhancing effects were comparable to those of DPZ, highlighting its potential as a promising therapeutic candidate for the management of cognitive impairments.

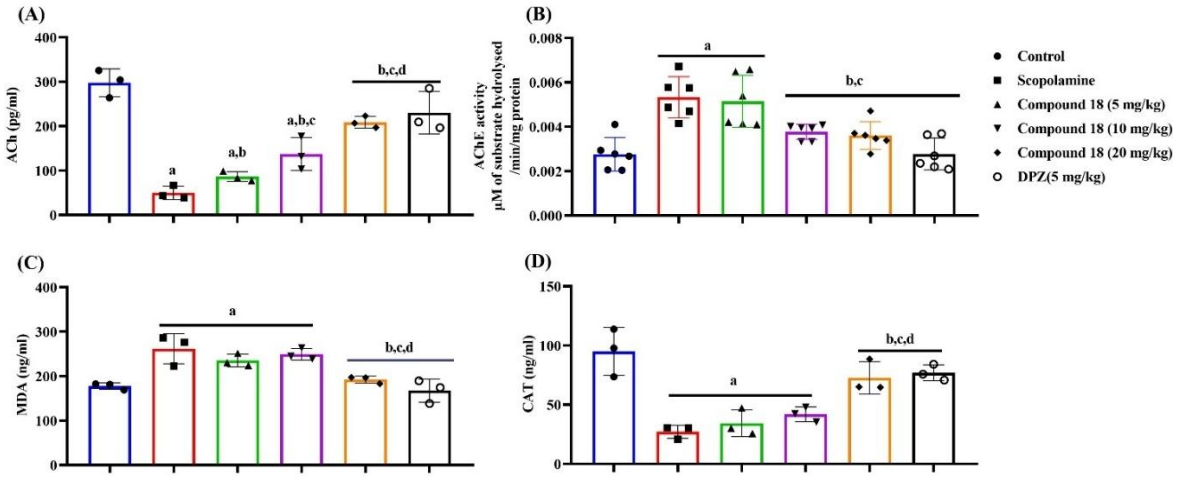

Figure 5.10. Effect of compound **18** on *ex vivo* biochemical parameters **(A)** ACh activity, (B) AChE activity, **(C)** Measurement of MDA activity and **(D)** Measurement of CAT levels. $^{a}P < 0.05$ vs. control; $^{b}P < 0.05$ vs. scopolamine; $^{c}P < 0.05$ vs compound **18** (5 mg/kg); $^{d}P < 0.05$ vs. compound **18** (10 mg/kg).

5.4 Summary and conclusion

Theranostic agents for AD were developed with potential to simultaneously perform detection of Aβ species and inhibit cholinesterase (ChEs) enzymes, which are primary targets in the development of AD therapeutics. The agents were constructed utilizing structural features from the anti-AD molecules and the fluoroprobes with the architecture of an electron donor-acceptor. Indolium and benzothiazolium were used as fluorophores and were combined with substituted *N*-aryl piperazine scaffold having proven therapeutic activity against AD. The compound/probe **18** containing 2-pyridine substitution on piperazine scaffold exhibited significant inhibition ChEs (AChE; IC_{50} = 0.172 ± 0.011 μM; BuChE; IC_{50} = 1.376 ± 0.141 μM), indicating its therapeutic potential. Remarkable photophysical properties were produced by the synthesized probes. The enhancement in the fluorescence response upon binding of Probe **18** with $A\beta_{1\text{-}42}$ aggregates were observed in the binding study assay. The high affinity of probe **18** towards the $A\beta_{1\text{-}42}$ aggregates as established in the *in vitro* saturation binding assay (Kd = 0.731 μM). Probe **18** indicated

its ability to detect the Aβ deposit in *elavGAL4>UAS Aβ*, *Drosophila* model for AD, which was comparable with the standard Thioflavin T dyes. Compound **18** with potent ChEs inhibitory activity, significant fluorescent properties and potential to detect Aβ species was further evaluated for *in vivo* studies. It presented no sign of any toxicity, changes in body weight, alternations in food or water intake, and absence of mortality were observed following the administration of lead compound **18** in acute toxicity studies. Moreover, *in-vivo* behavioural studies of compound **18** demonstrated a significant improvement in cognitive and spatial memory deficits in the scopolamine-induced cognitive impairment mouse model. The *ex-vivo* analysis showed a reduction in the AChE and an increase in levels of ACh, indicated significant inhibition of brain AChE. The assessment of MDA and CAT showed the antioxidant potential of test compound **18**. Thus, compound/probe **18** demonstrated excellent properties as contrast fluorescent agent along with therapeutic activity in *in-vitro* and *in-vivo* evaluations, it emersed as a potential theranostic agent and a safe and effective lead for AD